MGL1109 Ocean Bottom Seismometer Profiles: Instrument Relocations and Preliminary Data Quality Assessment

Gail L. Christeson
University of Texas Institute for Geophysics

September 19, 2011

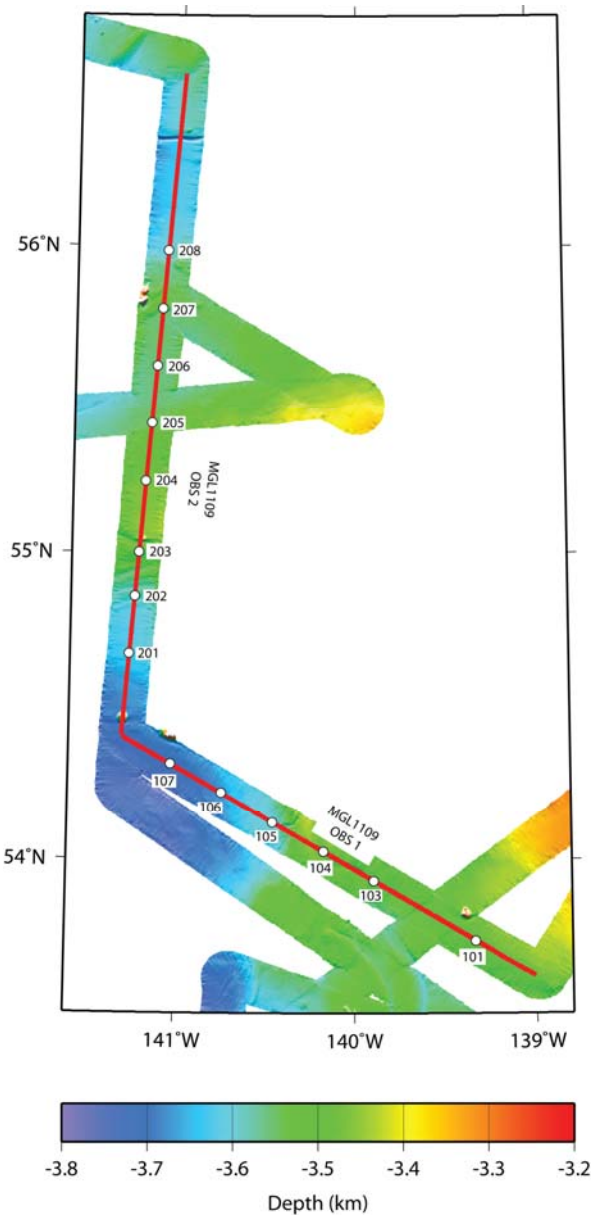

Fig. 1. Multibeam bathymetry along MGL1109 wide-angle profiles OBS1 and OBS2. 6 instruments were recovered along profile OBS1, and 8 were recovered along profile OBS2.

Study Area

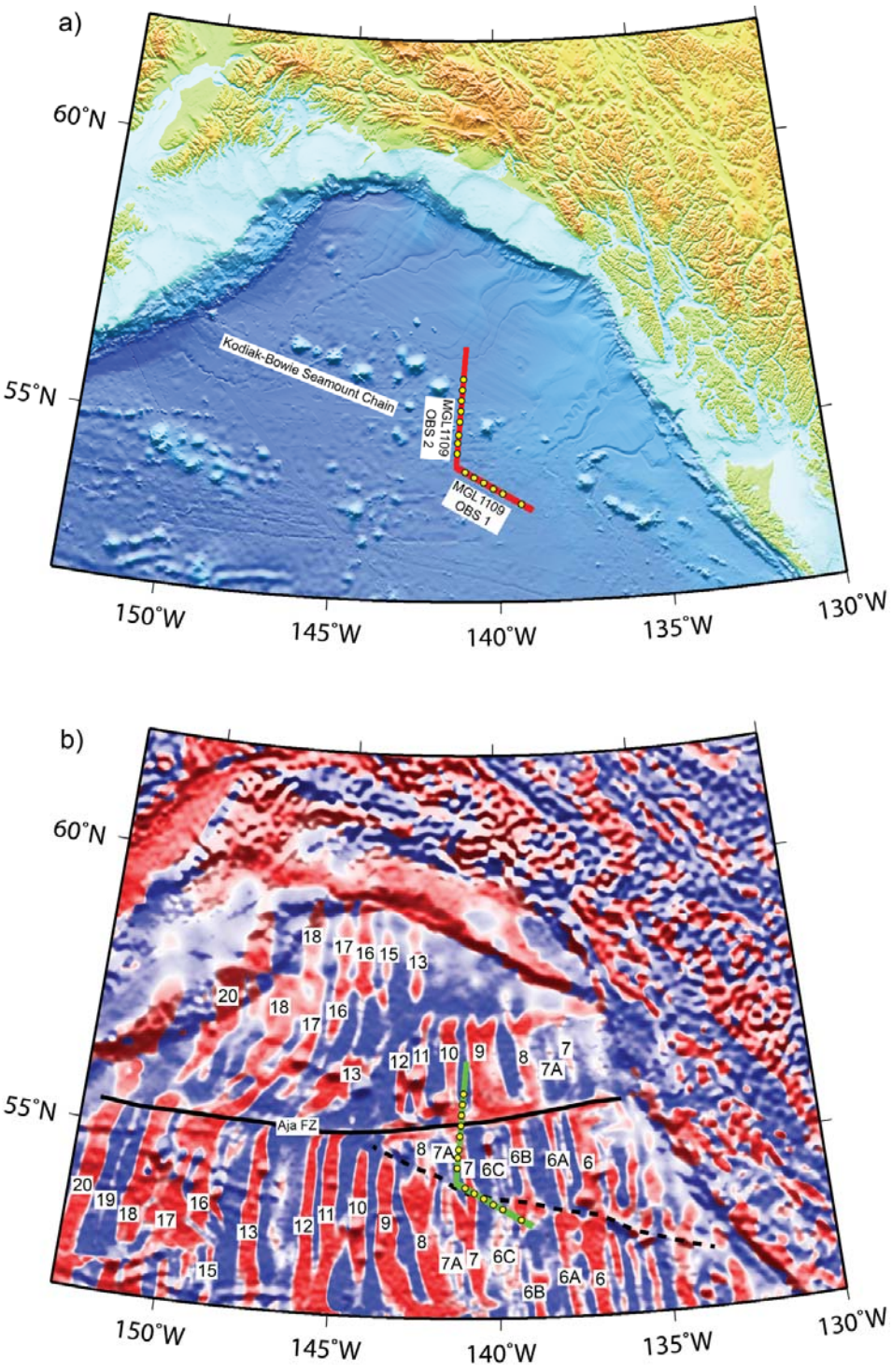

Fig. 2. a) Topography of the Gulf of Alaska study region. Seafloor bathymetry is from *Smith and Sandwell* [1997], and onshore topography is GTOPO30 from U.S. Geological Survey. b) EMAG2 magnetics of the Gulf of Alaska study region from CIRES. Anomaly identification is from *Atwater and Severinghaus* [1989]; the dashed line is identified as a wandering small offset.

Profiles OBS01 and OBS02 are located over sedimented 22-28 Ma oceanic crust in the Gulf of Alaska. Primary features observed in the bathymetry and magnetics (Fig. 2) are the Kodiak-Bowie seamount chain, the Aja fracture zone, and a disruption in the magnetics which is identified by *Atwater and Severinghaus* [1989] as a small wandering offset. Profile OBS01 is located near the trace of the small wandering offset; profile OBS02 crosses the Aja fracture zone and the Kodiak-Bowie seamount chain.

Instrument Relocation

The R/V *Norseman* science party recorded deployment and recovery positions for all OBSs. The instruments may be affected by currents while traveling through the water column, but horizontal movement is less likely to occur during descent to the seafloor because the instrument is attached to a metal anchor frame. Hence, seafloor positions of instruments are expected to be closer to deployment position than to recovery position. In addition, instruments will drift on the sea surface while the vessel maneuvers during retrieval operations.

For all instruments I inverted direct water wave arrivals to estimate instrument position on the seafloor. Initial positions were set to deployment positions; instrument depths were obtained from processed multibeam bathymetry acquired by the R/V *Langseth* (Fig. 1). Shot positions and times were generated by LDEO; shot depths were set to 9 m. The inversions placed the seafloor positions 55-200 m from deployment positions, with a mean difference of 115 m. Table 1 summarizes instrument positions, and Fig. 3 displays an example inversion.

Table 1. Deployment, recovery, and estimated seafloor OBS positions

OBS	Deployment	Recovery	Seafloor
101	53.7361, -139.329	53.7338, -139.3361	53.73663, -139.33188
102	53.8342, -139.611	no recovery	
103	53.9314, -139.891	53.935, -139.889	53.93119, -139.89228
104	54.02768, -140.1731	54.0291, -140.1713	54.02774, -140.17227
105	54.1237, -140.456	54.1264, -140.4558	54.12277, -140.45700
106	54.219, -140.741	54.2215, -140.742	54.21976, -140.74164
107	54.3135, -141.0268	54.3155, -141.0294	54.31416, -141.02825
201	54.6702, -141.2674	54.671, -141.2699	54.67113, -141.26884
202	54.8583, -141.241	54.8585, -141.245	54.85820, -141.23957
203	55.0019, -141.2207	55.0011, -141.2233	55.00133, -141.22096
204	55.2344, -141.1872	55.2333, -141.1895	55.23330, -141.18884
205	55.422, -141.16	55.4229, -141.1598	55.42188, -141.15829
206	55.6104, -141.1327	55.6112, -141.1357	55.60972, -141.13120
207	55.7982, -141.1051	55.797, -141.108	55.79715, -141.10451
208	55.9865, -141.0782	55.9862, -141.0782	55.98547, -141.07843

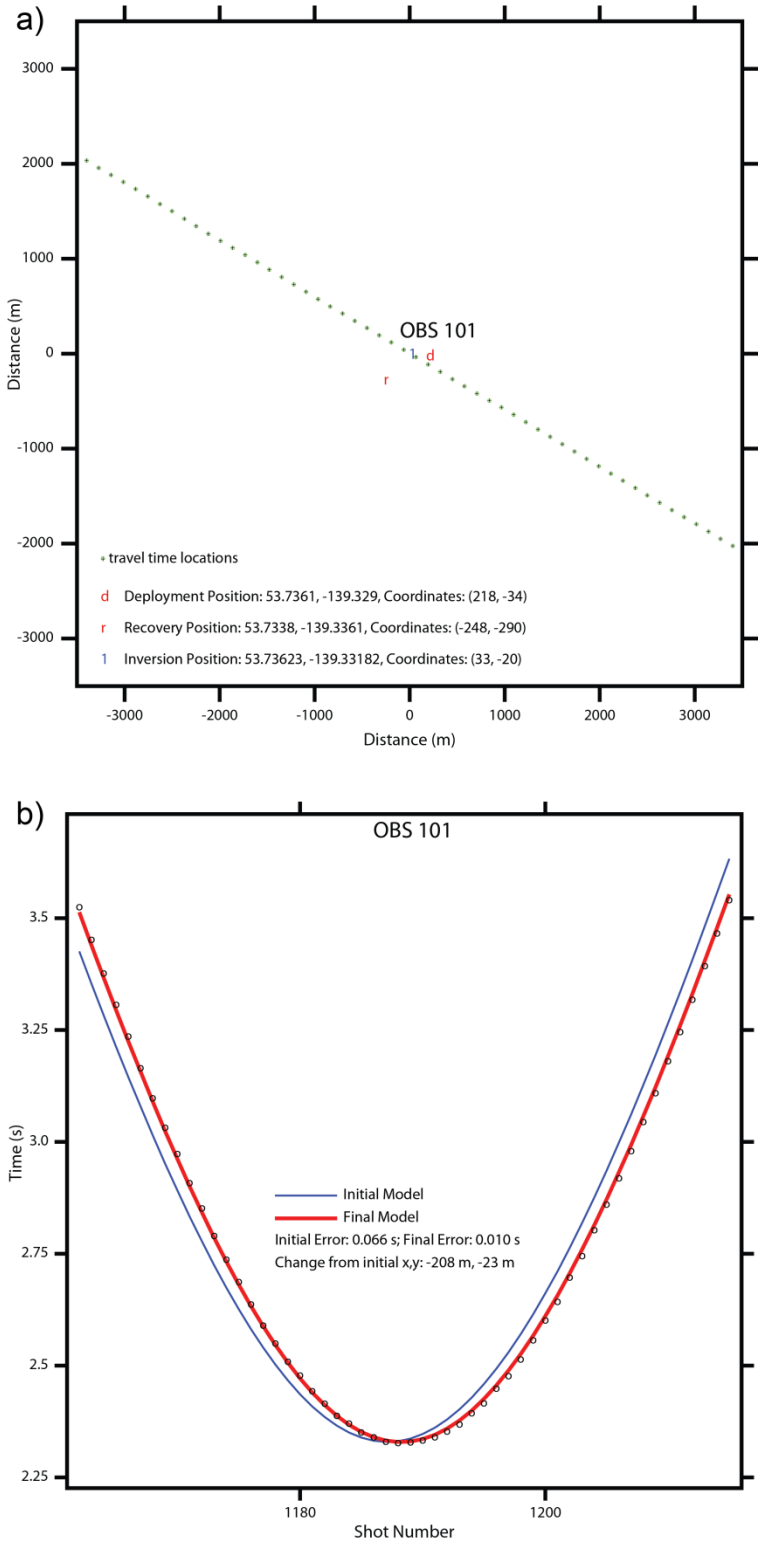

Fig. 3. a) Deployment, recovery, and estimated seafloor position of OBS 101. Green circles and crosses display shot positions; direct water wave travel times from these shots were inverted for position of instrument on seafloor. b) Calculated water wave travel times from shots to instrument for deployment position (blue) and estimated seafloor position (red).

Record Sections

All recovered OBSs recorded excellent hydrophone and vertical channel data, with the exception of OBS 103 where the vertical data were poor. Fig. 4 displays example data for OBS 101. At near offsets (Fig. 4a) prominent arrivals include the direct water wave, sediment refractions, reflections from the basement, and basement refractions (Pg phase). At far offsets (Fig. 4b) a prominent PmP is observed at offsets of 25-60 km, with Pn observed breaking from the PmP arrival at ofsets of 40-75 km. Fig. 5 and Fig. 6 display record sections for all instruments.

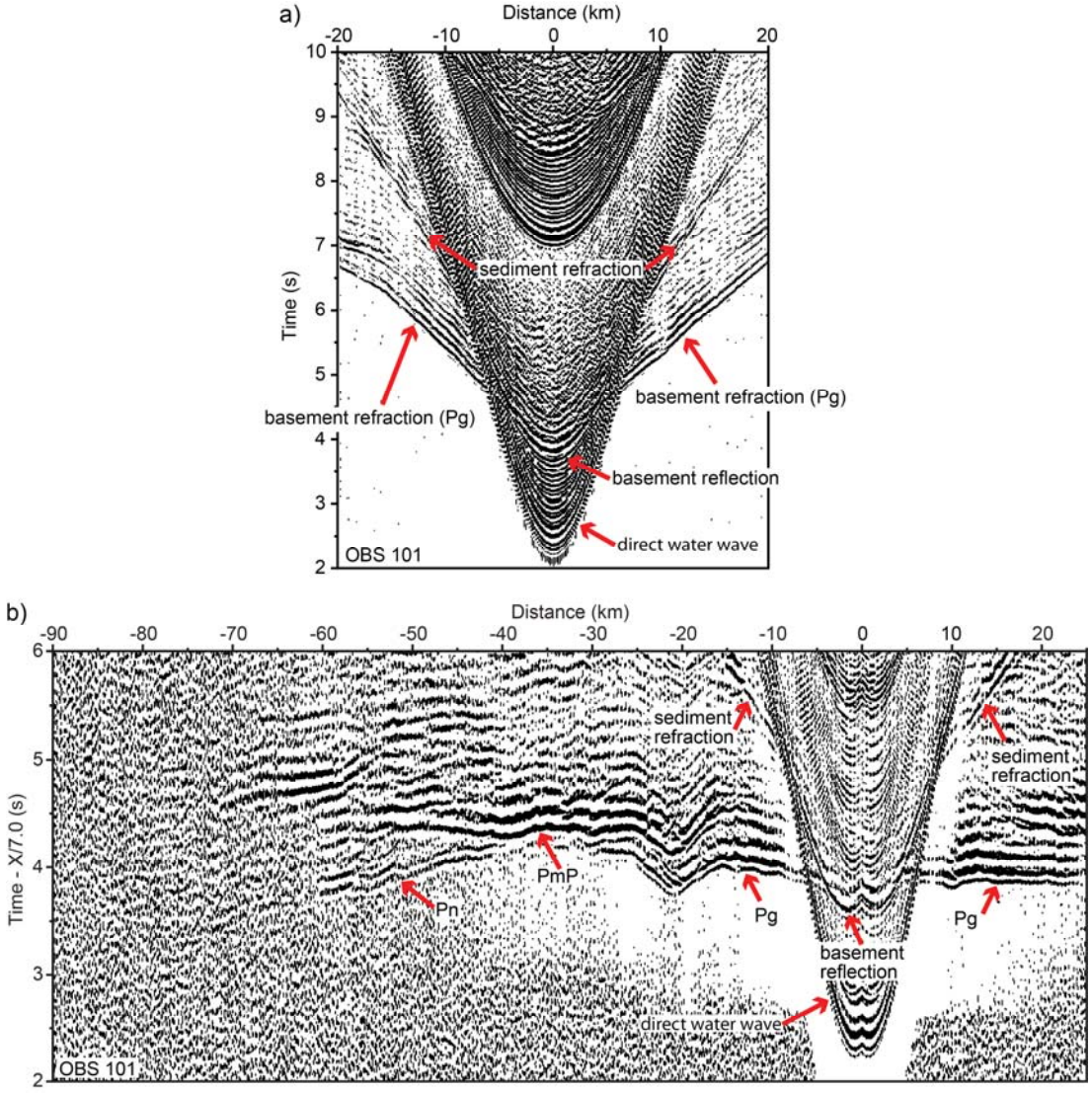

Fig. 4. a) Near offset arrivals on hydrophone channel of OBS 101. Record section is plotted with range scaling by a factor of $R^{1.0}$, where R is the distance of the shot from the receiver. b) Record section for vertical channel of OBS 101. Data are plotted with a reduction velocity of 7 km/s, and have an 0.5-second agc applied. Data for both record sections are bandpass filtered with a low cut of 3 Hz and a high cut of 15 Hz. Prominent arrivals are identified.

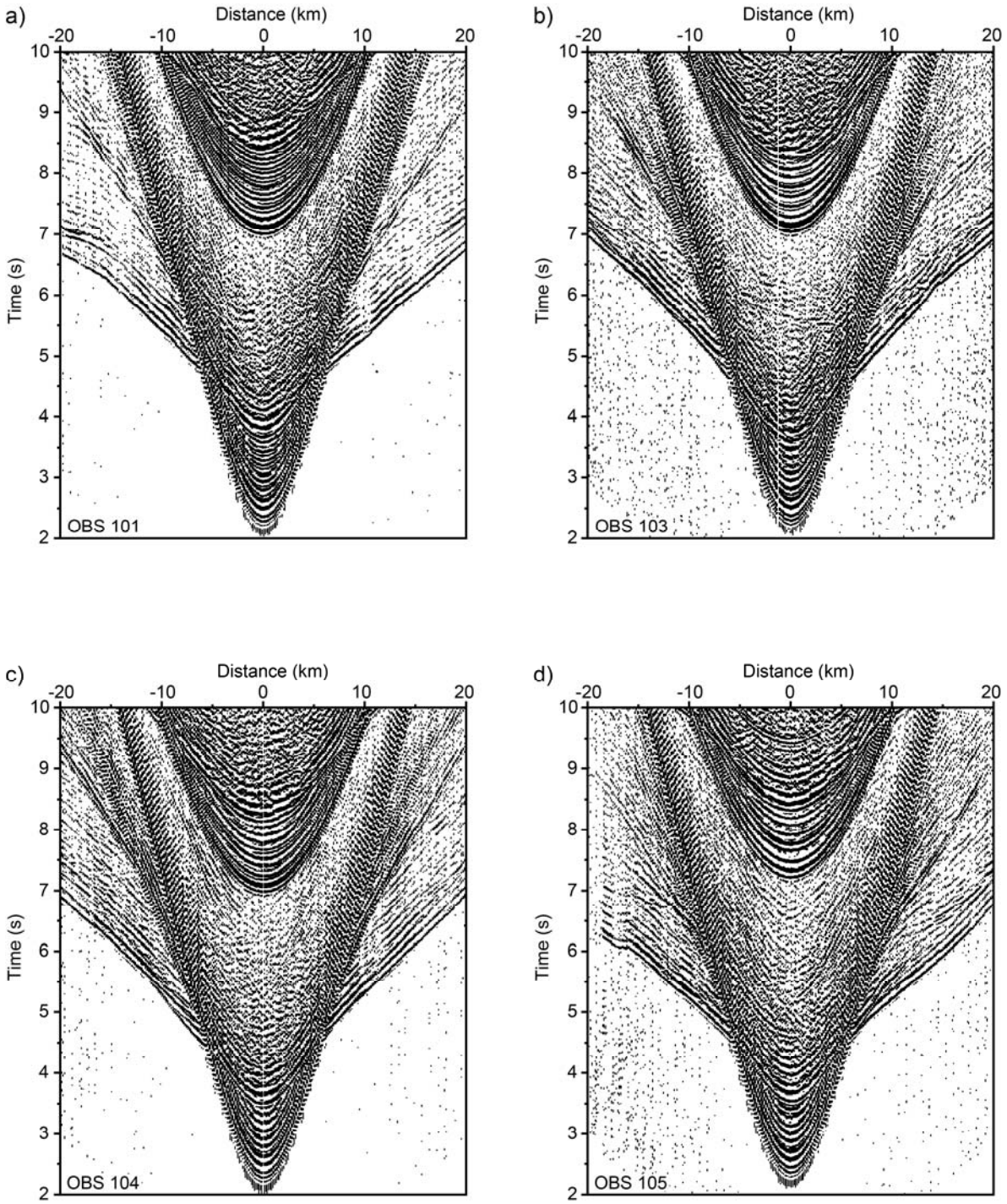

Fig. 5. Near offset arrivals on hydrophone channel for all instruments. Record sections are plotted with range scaling by a factor of $R^{1.0}$, where R is the distance of the shot from the receiver. Data are bandpass filtered with a low cut of 3 Hz and a high cut of 15 Hz.

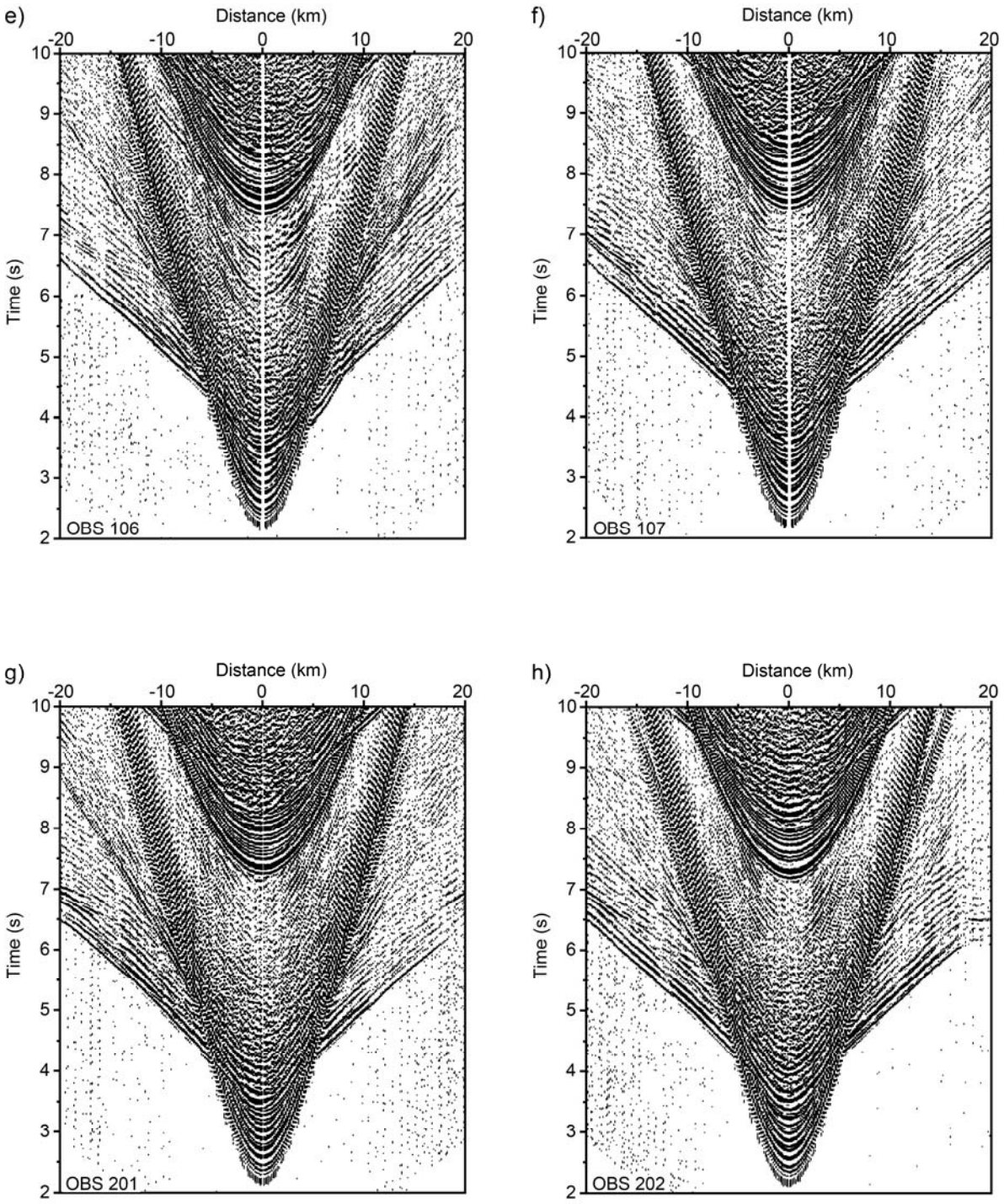
e)
Distance (km)
-20
-10
0
10
20
Time (s)
10
9
8
7
6
5
4
3
2
OBS 106
f)
Distance (km)
OBS 107
g)
Distance (km)
OBS 201
h)
Distance (km)
OBS 202

Fig. 5, cont.

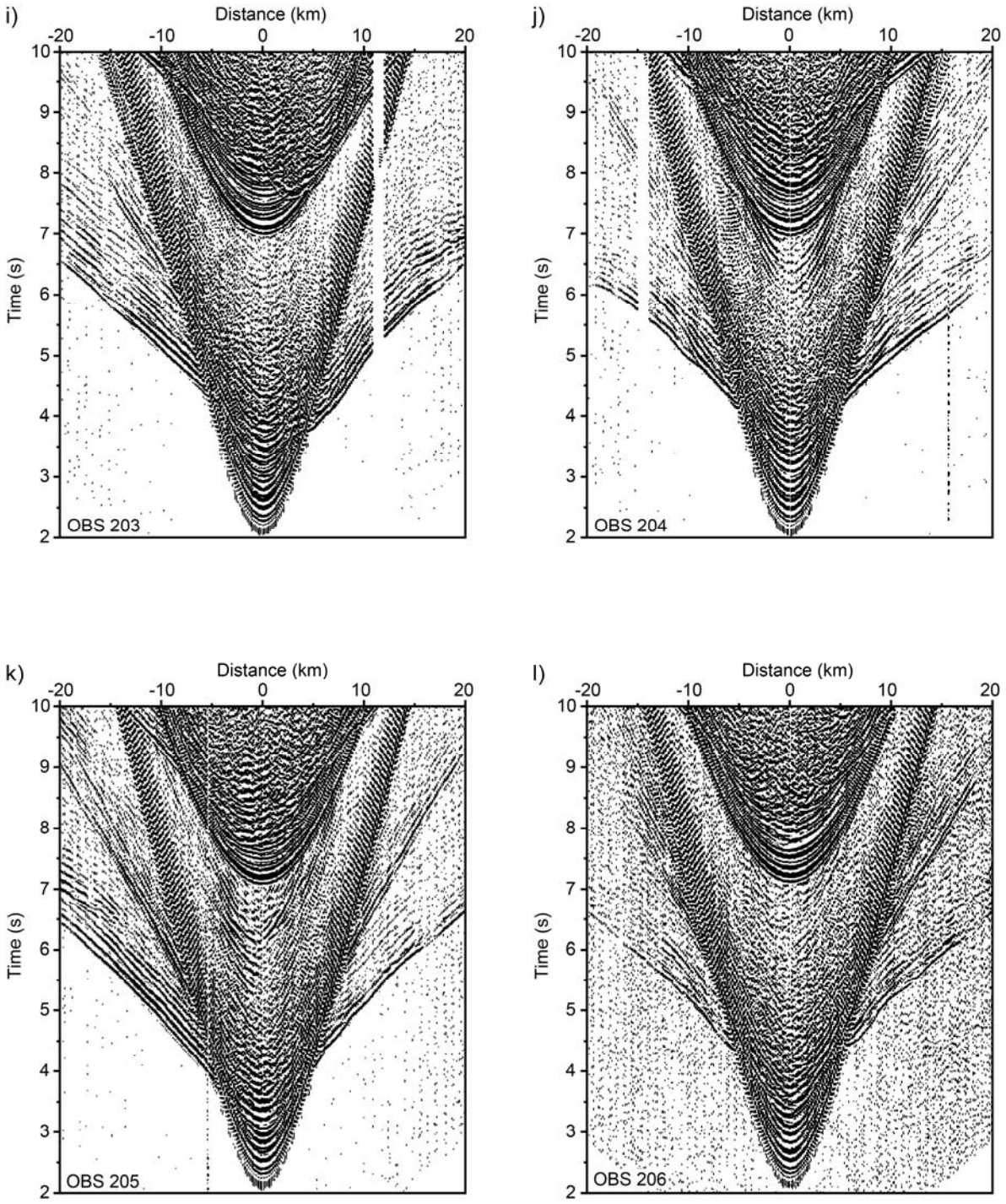
i)
Distance (km)
-20
-10
0
10
20
Time (s)
2
3
4
5
6
7
8
9
10
OBS 203
j)
Distance (km)
OBS 204
k)
Distance (km)
OBS 205
l)
Distance (km)
OBS 206

Fig. 5, cont.

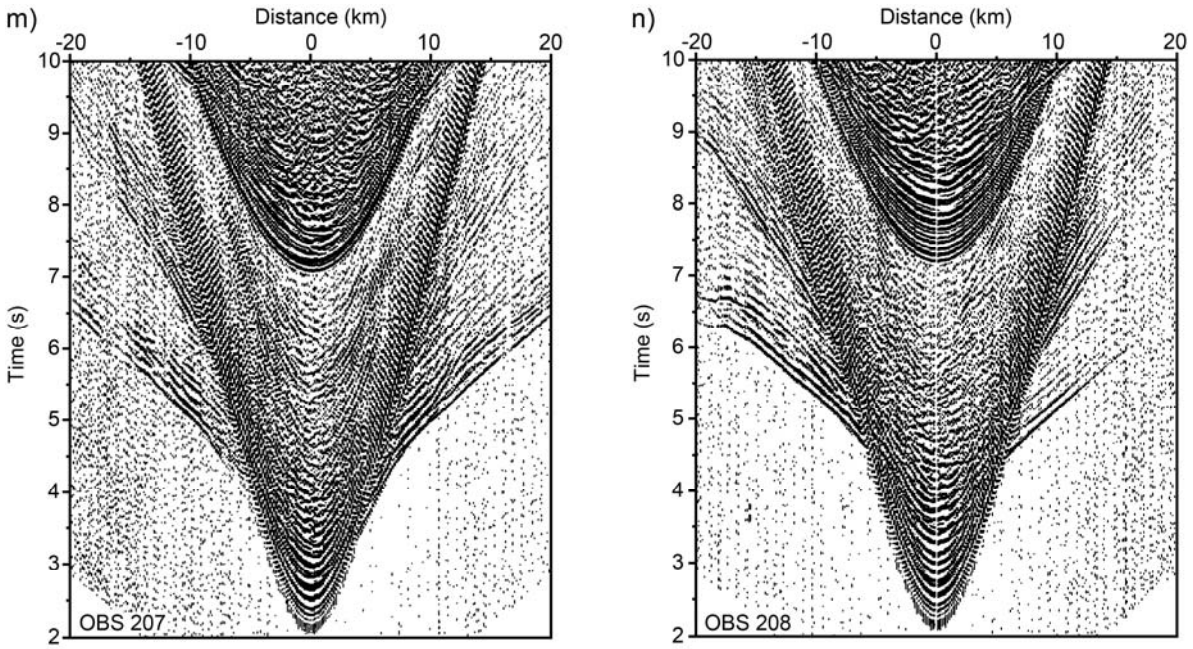
m)
Distance (km)
-20
-10
0
10
20
Time (s)
2
3
4
5
6
7
8
9
10
OBS 207
n)
Distance (km)
-20
-10
0
10
20
Time (s)
2
3
4
5
6
7
8
9
10
OBS 208

Fig. 5, cont.

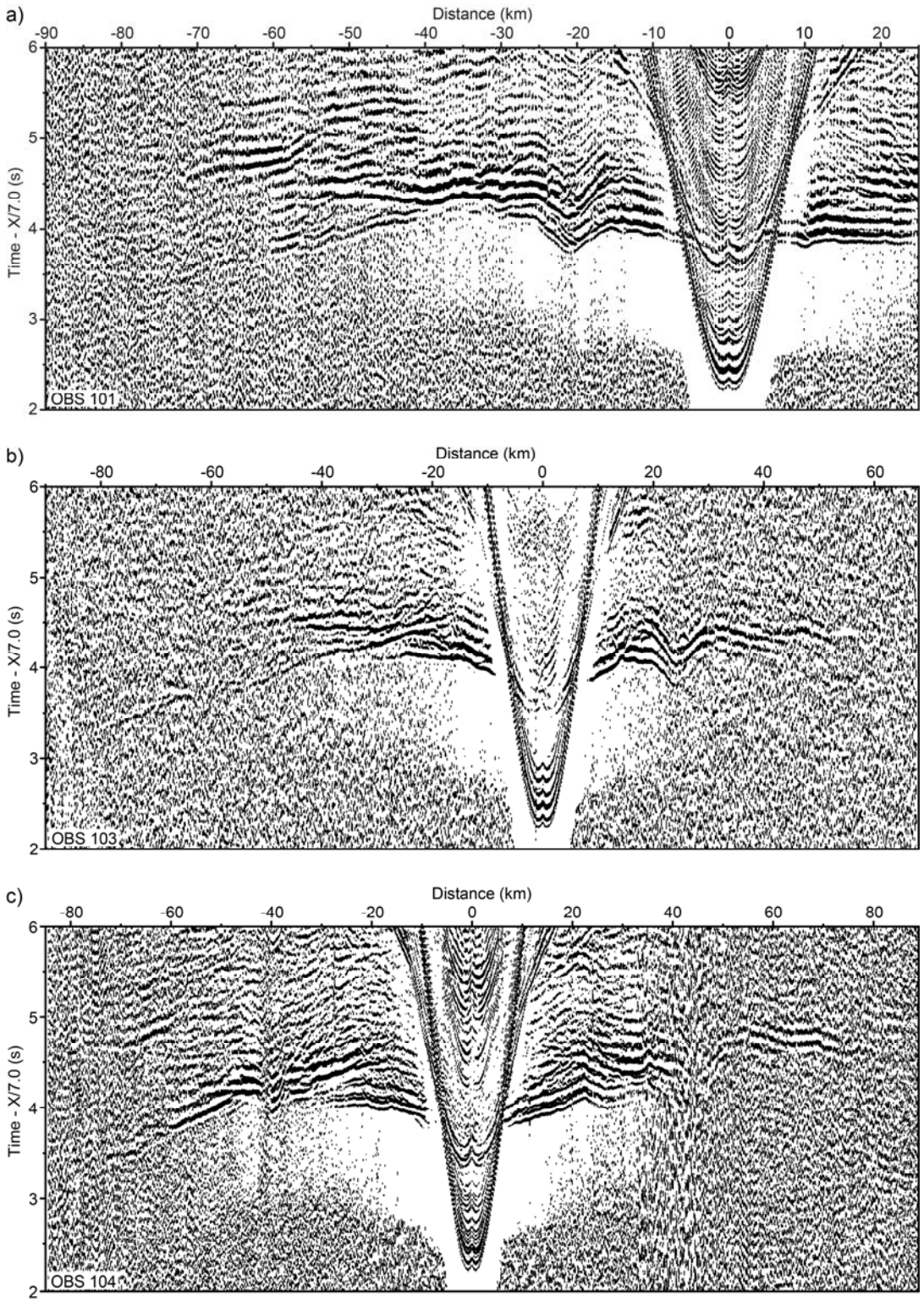

Fig. 6. Record sections for all instruments. Vertical channel is displayed for all OBSs except OBS103 where the hydrophone channel is shown. Data are plotted with a reduction velocity of 7 km/s, and have an 0.5-second agc applied. Data are bandpass filtered with a low cut of 3 Hz and a high cut of 15 Hz.

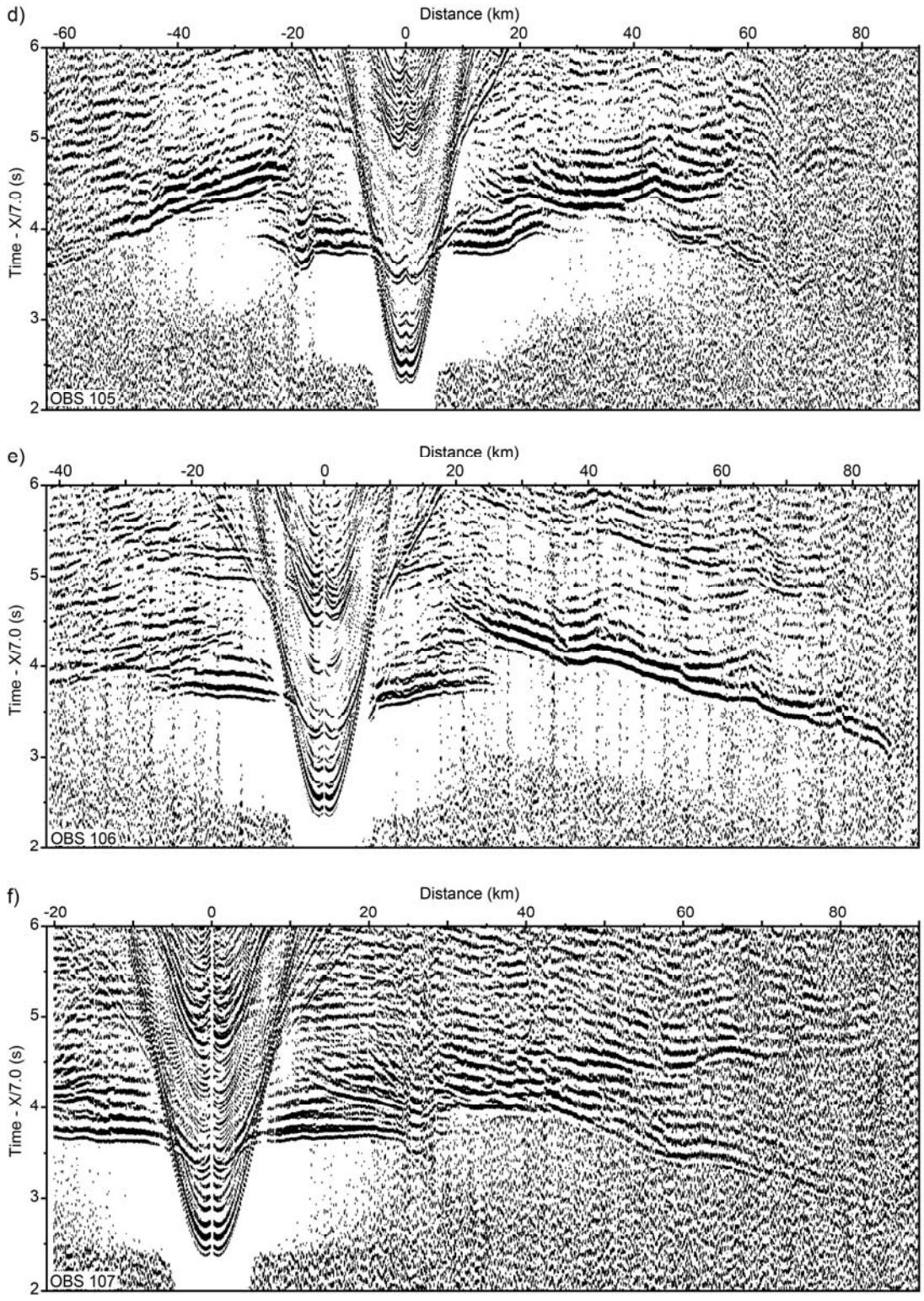
d)
Distance (km)
-60
-40
-20
0
20
40
60
80
6
5
4
3
2
Time - X/7.0 (s)
OBS 105
e)
Distance (km)
-40
-20
0
20
40
60
80
6
5
4
3
2
Time - X/7.0 (s)
OBS 106
f)
Distance (km)
-20
0
20
40
60
80
6
5
4
3
2
Time - X/7.0 (s)
OBS 107

Fig. 6, cont.

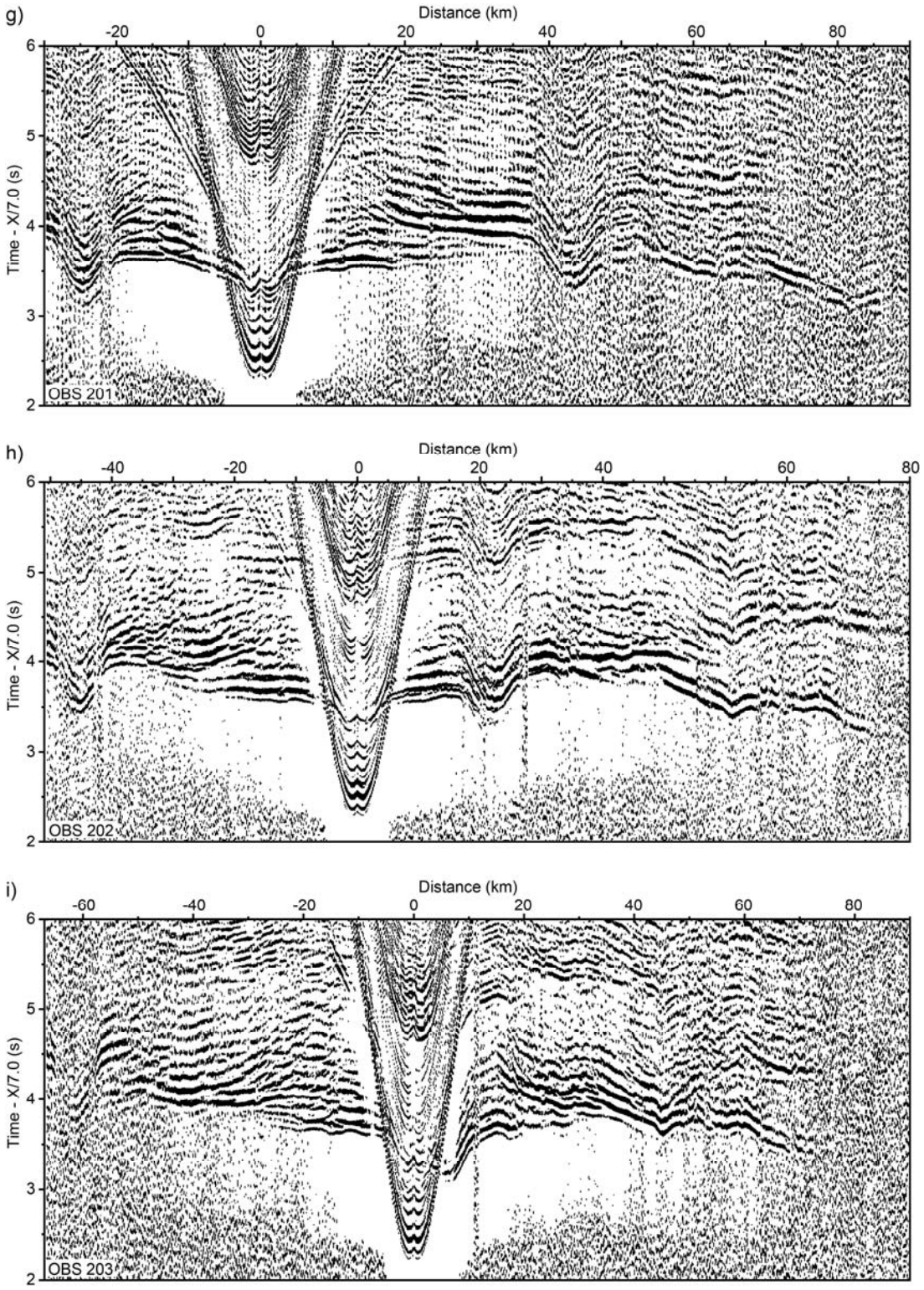
g)
Distance (km)
-20
0
20
40
60
80
6
5
4
3
2
Time - X/7.0 (s)
OBS 201
h)
Distance (km)
-40
-20
0
20
40
60
80
6
5
4
3
2
Time - X/7.0 (s)
OBS 202
i)
Distance (km)
-60
-40
-20
0
20
40
60
80
6
5
4
3
2
Time - X/7.0 (s)
OBS 203

Fig. 6, cont.

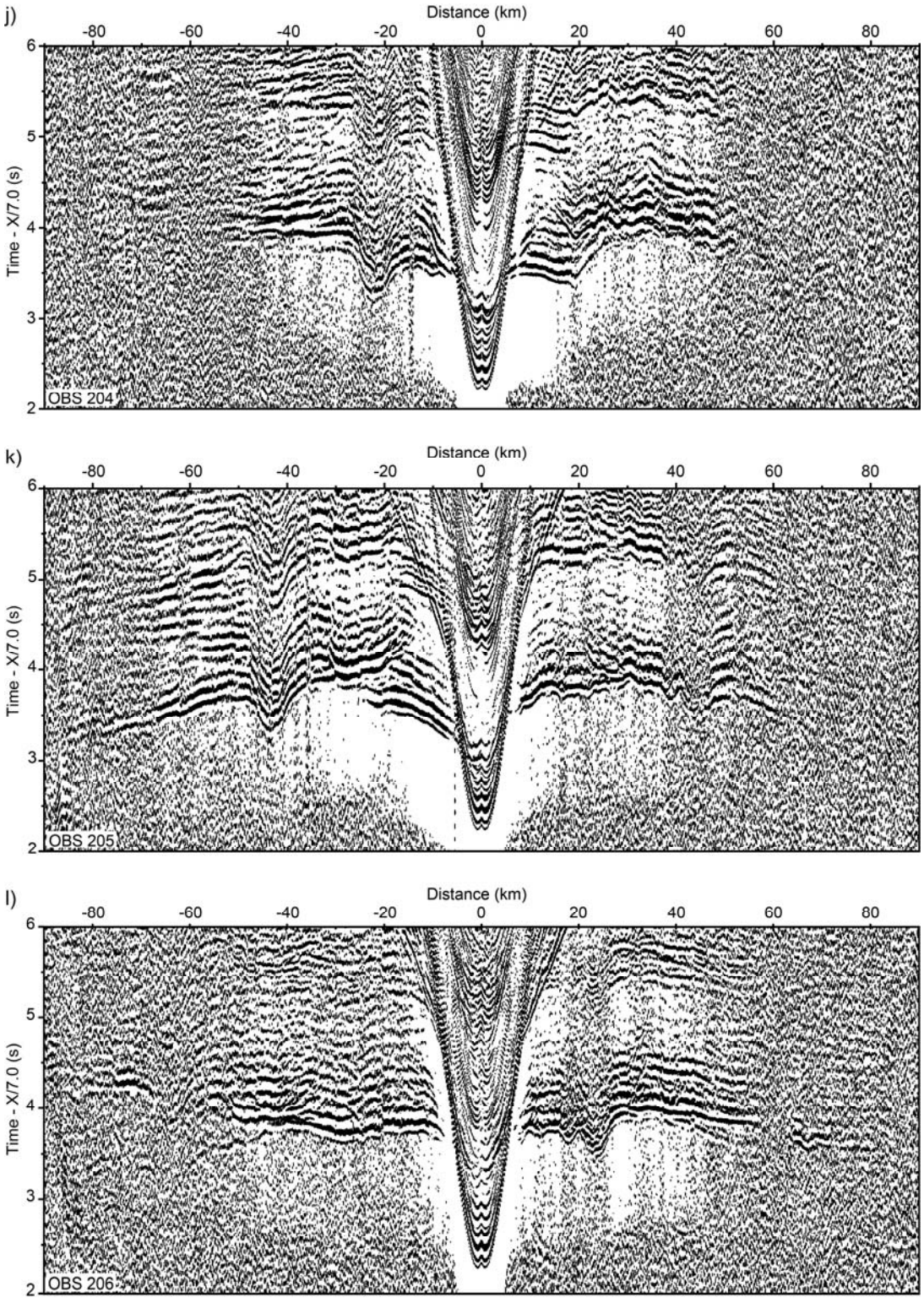
j)
Distance (km)
-80
-60
-40
-20
0
20
40
60
80
6
5
4
3
2
Time - X/7.0 (s)
OBS 204
k)
Distance (km)
-80
-60
-40
-20
0
20
40
60
80
6
5
4
3
2
Time - X/7.0 (s)
OBS 205
l)
Distance (km)
-80
-60
-40
-20
0
20
40
60
80
6
5
4
3
2
Time - X/7.0 (s)
OBS 206

Fig. 6, cont.

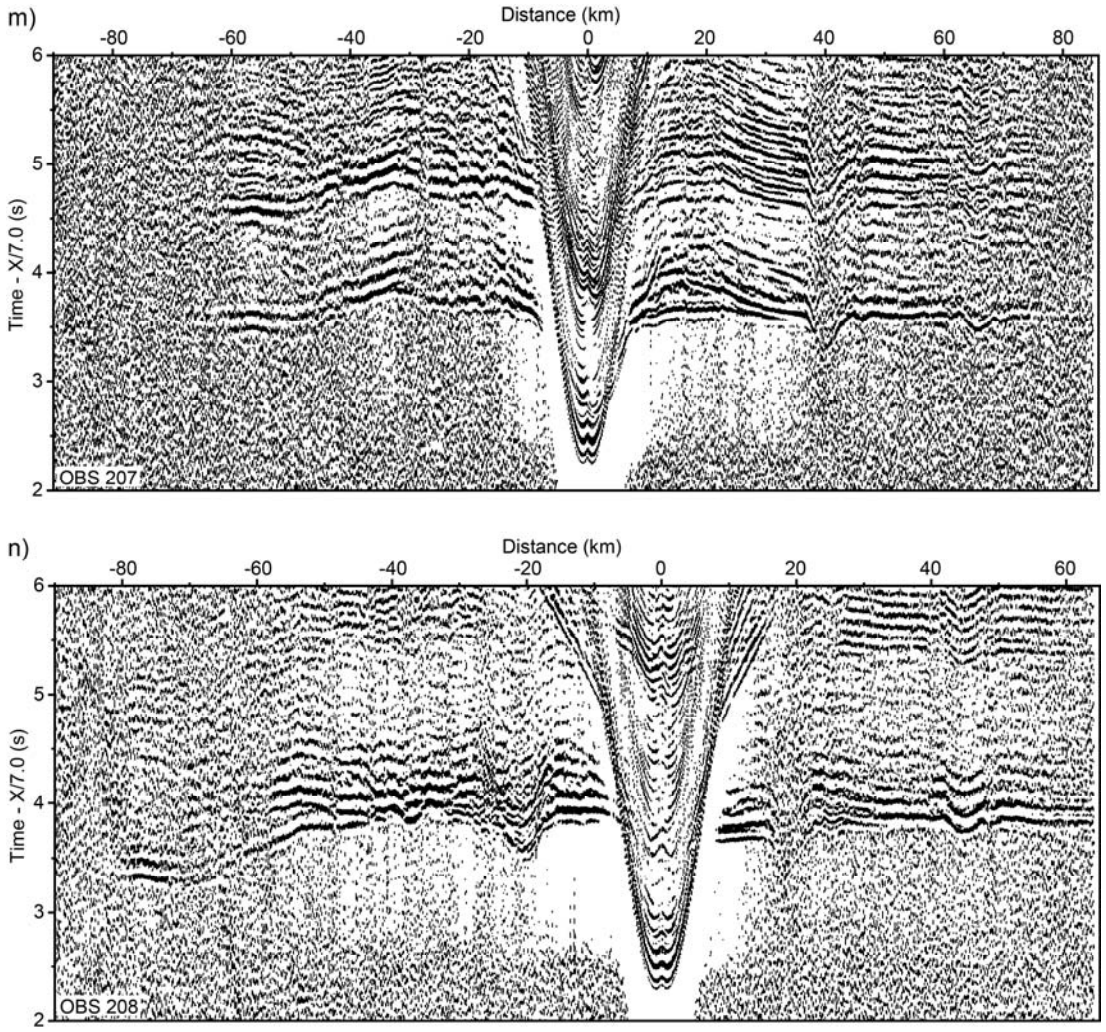
m)
Distance (km)
-80
-60
-40
-20
0
20
40
60
80
6
5
4
3
2
Time - X/7.0 (s)
OBS 207
n)
Distance (km)
-80
-60
-40
-20
0
20
40
60
6
5
4
3
2
Time - X/7.0 (s)
OBS 208

Fig. 6, cont.

References

Atwater, T., and J. Severinghaus (1989), Tectonic maps of the northeast Pacific, in *Decade of North American Geology, vol. N, The Eastern Pacific Ocean and Hawaii*, edited by E. L. Winterer, D. M. Hussong and R. W. Decker, pp. 15-20.

Smith, W. H. F., and D. T. Sandwell (1997), Global sea floor topography from satellite altimetry and ship depth soundings, *Science*, *277*, 1956-1962, 10.1126/science.277.5334.1956: 10.1126/science.277.5334.1956.